scientific reports

Check for updates

OPEN

Triple synergistic enhancement of breast cancer treatment via chemotherapy, chemodynamic therapy, and tumor starvation therapy driven by lipid-COF nanoparticles

Yiya Sun[1,6], Zhenkun Ren[3,6], Zhiruo Zhang[2], Kexin Yang[2], Yufan Jin[2], Hanyu Deng[2], Yingzi Liu[4], Jiali Wang[4], Peng Ji[2,5]✉ & Peng Liu[1]✉

In this study, a novel cascade nano delivery system, Cur/Gox@LCOF, was developed for enhanced breast cancer therapy. The system loads curcumin (Cur) and glucose oxidase (Gox) into a lipid copper-based organic framework (LCOF) carrier for enhanced tumor therapy. The nanoparticles were characterized by X-ray diffraction (XRD), transmission electron microscopy (TEM), and dynamic light scattering (DLS), which showed that they had a uniform spherical morphology with an average particle size of about 80 nm, displaying stable colloidal properties. The system showed excellent stability under simulated physiological conditions and exhibited pH-responsive drug release properties, contributing to the controlled release of Cur and Gox. The results of in vitro cellular experiments showed that Cur/Gox@LCOF significantly enhanced the production of reactive oxygen species (ROS), leading to significant cytotoxicity in cancer cells. In addition, the system also demonstrated enhanced therapeutic efficacy and good biocompatibility in a tumor mouse model. Thus, this study developed a nanocarrier platform for triple synergistic chemokinetic/chemotherapy/starvation therapy, which has promising applications in the efficient treatment of tumors.

Keywords Copper framework, Chemodynamic therapy, Curcumin, Glucose oxidase, Breast cancer

Breast cancer represents one of the most prevalent malignancies among women globally, with its incidence steadily increasing in recent years[1]. In 2020, the number of newly diagnosed breast cancer cases reached 2.26 million worldwide, surpassing lung cancer for the first time to become the most frequently occurring cancer type[2]. Characterized by complex pathological features and significant heterogeneity, breast cancer not only exhibits a high incidence rate but also poses a considerable threat to women's health, making it a critical focus of contemporary oncological research. Current therapeutic approaches, including surgery, radiotherapy, chemotherapy, targeted therapy, and immunotherapy, are widely employed; however, these modalities are frequently associated with significant limitations, such as severe toxic side effects, multidrug resistance, tumor recurrence, and metastasis[3]. These challenges substantially hinder therapeutic outcomes and adversely affect patients' quality of life. Consequently, the development of innovative therapeutic strategies that offer enhanced efficacy with reduced toxicity has become a pivotal objective in advancing breast cancer treatment and improving patient prognoses[4].

In recent years, the rapid advancements in biotechnology have catalyzed the emergence of multimodal combined targeted therapy as a promising strategy for cancer treatment. Unlike monotherapies, multimodal approaches target tumor progression through multiple mechanisms, enhancing therapeutic efficacy while

[1]The First Affiliated Hospital of Jinzhou Medical University, Jin Zhou 121000, China. [2]College of Pharmacy and Chemistry & Chemical Engineering, Taizhou University, Taizhou 225300, China. [3]The Third Affiliated Hospital of Jinzhou Medical University, Jin Zhou 121000, China. [4]Jinzhou Medical University, Jinzhou 121000, China. [5]Liangzhu Laboratory, Zhejiang University School of Medicine, Hangzhou 310000, PR China. [6]Yiya Sun and Zhenkun Ren contributed equally. ✉email: jipeng0213@163.com; liup@jzmu.edu.cn

minimizing damage to normal tissues[5]. Among these, chemodynamic therapy (CDT) has gained attention as an innovative modality that utilizes metal ions to catalyze endogenous hydrogen peroxide (H_2O_2) in the tumor microenvironment, generating highly cytotoxic reactive oxygen species (ROS), such as hydroxyl radicals (•OH)[6]. This process enables selective tumor cell eradication and offers high therapeutic specificity[7]. Despite its potential, CDT faces significant challenges in clinical application[8,9]. First, the low concentration of H_2O_2 in the tumor microenvironment limits the generation of sufficient •OH. Second, the elevated levels of glutathione (GSH) in tumor cells attenuate the catalytic efficiency of CDT. Addressing these obstacles through the development of highly targeted strategies to enhance H_2O_2 availability and deplete GSH is critical for improving the therapeutic outcomes of CDT.

Nanometal-organic frameworks (nMOFs) have garnered significant attention in the field of CDT owing to their distinctive structural attributes[10]. Constructed from inorganic metal nodes and organic bridging ligands, nMOFs exhibit high porosity, a large specific surface area, and excellent biocompatibility, making them highly suitable platforms for tumor-targeted drug delivery and catalytic therapies. Among various nMOFs, copper-based nMOFs (Cu-nMOFs) have emerged as a focal point of research due to their exceptional Fenton-like catalytic activity under neutral and weakly acidic conditions[9,11]. Cu^{2+} ions not only catalyze the decomposition of H_2O_2 to produce •OH but also deplete intracellular GSH through redox reactions, thereby amplifying oxidative stress and enhancing anti-tumor efficacy. Furthermore, Cu^{2+} exhibits a significantly higher reaction rate compared to Fe^{2+} in traditional Fenton reactions, enabling more efficient tumor cell eradication. These attributes position Cu-nMOFs as a promising platform for CDT, offering a novel and effective approach to breast cancer therapy.

The incorporation of glucose oxidase (GOx) into CDT systems offers a powerful strategy to enhance therapeutic outcomes[12]. GOx, a natural oxidoreductase, efficiently catalyzes the oxidation of glucose to generate H_2O_2, thereby increasing H_2O_2 levels within the tumor microenvironment and providing an abundant substrate for Fenton-like reactions[4]. Studies demonstrate that the combination of GOx with iron-based or copper-based Fenton reagents significantly amplifies ROS production, resulting in enhanced tumor cytotoxicity[11]. Furthermore, by depleting glucose during its catalytic process, GOx disrupts the energy supply to tumor cells, inducing apoptosis and necrosis. The synergistic integration of Cu-nMOFs with GOx effectively improves the an-ti-breast cancer efficacy of CDT by simultaneously enhancing H_2O_2 production, depleting GSH, and intensifying oxidative stress. This multifaceted therapeutic approach represents a promising avenue for precision breast cancer treatment, with broad potential for clinical application.

In this study, a cascade Cu-nMOFs nano drug delivery system (Cur/Gox@LCOF, Fig. 1) was designed and developed to achieve triple synergistic anti-tumor effects through CDT, chemotherapy, and starvation therapy. This system employs COF as both a copper source and a carrier for curcumin (Cur) and GOx. To enhance biocompatibility and prevent premature drug leakage during systemic circulation, the nano platform is encapsulated with a lipid coating. Benefiting from the enhanced permeability and retention (EPR) effect, Cur/Gox@LCOF is efficiently accumulated in tumor tissues and subsequently degraded in the acidic tumor microenvironment, releasing Cu^{2+}, GOx, and Cur. GOx catalyzes glucose oxidation to produce H_2O_2, supplying a substrate for the Cu^{2}-mediated Fenton-like reaction while simultaneously disrupting tumor cell energy metabolism through starvation therapy. Additionally, the redox reaction between Cu^{2+} and glutathione (GSH) depletes the tumor's antioxidant capacity, further enhancing the efficacy of CDT. By integrating GOx-driven starvation therapy, GSH depletion-augmented CDT, and Cur-mediated chemotherapy, Cur/Gox@LCOF demonstrates a robust and safe anti-tumor effect, offering significant potential for clinical translation.

Results and discussion

Morphological and structural characterization of Cur/Gox@LCOF

COF, a widely utilized carrier in drug delivery systems, was synthesized through a straightforward one-step hydrothermal approach with minor modifications[13]. The synthesis procedures for both COF and Cur/Gox@LCOF were conducted as outlined in the schematic representation provided in Fig. 2A. X-ray diffraction (XRD) serves as a pivotal analytical technique for characterizing the crystal structures of materials. The XRD analysis of the synthesized COFs was performed, and the resulting diffraction pattern is presented in Fig. 2B. Characteristic peaks at $2\theta = 36.4°$ and 42.6° were observed, aligning well with previously reported data in the literature[14], thereby confirming the successful synthesis of the COF. Optical photographs (Fig. 2C) showed that the COF solution was blue-black, which is in agreement with the literature description[14], whereas the Cur/Gox@LCOF solution was yellow-black. The color difference provides evidence for the successful preparation of Cur/Gox@LCOF. The structural integrity and morphological characteristics of the synthesized COF and Cur/Gox@LCOF were systematically evaluated using transmission electron microscopy (TEM) and dynamic light scattering (DLS). DLS analysis revealed that the COF exhibited a hydrodynamic diameter of approximately 70 nm (Fig. 2D). Upon encapsulation of Cur and Gox within the liposomal COF structure, the hydrodynamic diameter increased to approximately 80 nm (Fig. 2E), indicating successful loading of the therapeutic agents. TEM imaging further confirmed that Cur/Gox@LCOF maintained a uniform spherical morphology with an average diameter of approximately 60 nm (Fig. 2F), supporting the structural stability of the nanosystem. Furthermore, the surface charge shifted from 4.14 mV for COF to −6.33 mV for Cur/Gox@LCOF following the encapsulation of Gox and liposome modification (Fig. 2G). The negative surface charge enhances colloidal stability and reduces aggregation, which, coupled with the optimized nanoparticle size, renders Cur/Gox@LCOF suitable for both in vitro and in vivo applications[15]. The aforementioned results provide preliminary evidence supporting the successful encapsulation of Gox into COF through cavity encapsulation and chelation of unliganded copper ions, as well as the successful synthesis of the Cur/Gox@LCOF formulation. A standard curve for Cur was constructed using UV spectrophotometry (equation: $y = 0.12386x + 0.03103$, $R^2 = 0.9973$; see Fig. 3A), while a standard curve for GOx was established through a BCA protein assay (equation: $y = 0.80926x + 0.1202$, $R^2 = 0.9999$; see Fig. 3B). Following the degradation of the core structure of Cur/Gox@LCOF nanoparticles, the drug loading (DL)

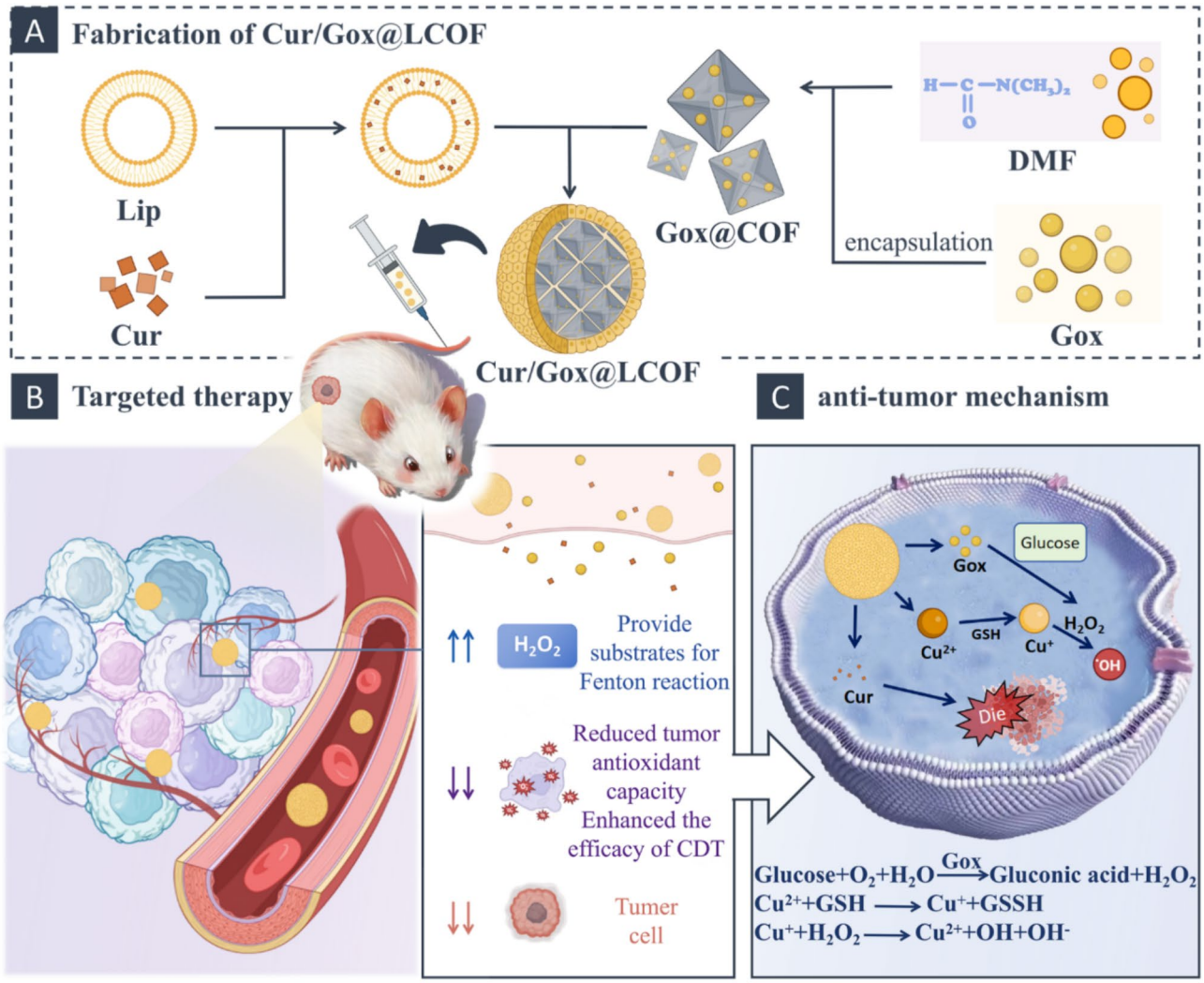

Fig. 1. Schematic diagram of the preparation process of the Cur/Gox@LCOF nano platform and its multimodal anti-tumor therapeutic mechanism.

efficiencies of Cur and Gox were determined to be 4.52% and 8.98%, respectively, demonstrating high loading capacities, which are adequate for subsequent experimental applications.

Stability studies

This study investigated the stability of the Cur/Gox@LCOF formulation under simulated physiological conditions, focusing on the release and degradation behavior of Cur at different temperature settings. The experimental results demonstrated that the Cur/Gox@LCOF formulation exhibited favorable stability at both 4 ℃ and 37 ℃. Notably, at 37 ℃, Cur/Gox@LCOF significantly enhanced the stability of Cur in comparison to free Cur. As depicted in Fig. 3C, at 4 ℃, although the Cur content in both formulations gradually decreased, it remained consistently above 95%, indicating that the Cur/Gox@LCOF formulation effectively protects Cur, preserving its stability. At the higher temperature of 37 ℃, the degradation rate of free Cur was notably higher than that of the Cur/Gox@LCOF formulation, which exhibited a slower degradation profile. These findings are in agreement with previous studies, highlighting that the encapsulation of drugs in nanocarriers can significantly attenuate their degradation rates, thereby improving both stability and bioavailability in vivo[16]. Specifically, it has been shown that nanocarriers, such as liposomes and metal-organic frameworks (MOFs), can efficiently shield drugs from direct exposure to the external environment, thereby prolonging the drug release period and reducing degradation[17,18]. The Cur/Gox@LCOF formulation demonstrated a marked improvement in Cur stability through encapsulation by nanocarriers, attributed to the unique structural and surface properties of the carrier. In particular, the liposomal layer and MOF structure together minimize curcumin's exposure to external factors, effectively reducing enzymatic degradation[19]. Additionally, the presence of the liposomal layer not only enhances the biocompatibility of Cur but may also further augment its therapeutic efficacy by decreasing its metabolic and clearance rates[20,21]. These findings suggest that the Cur/Gox@LCOF formulation holds promise for enhancing Cur's biological effects and stability, particularly in the context of long-term therapeutic applications.

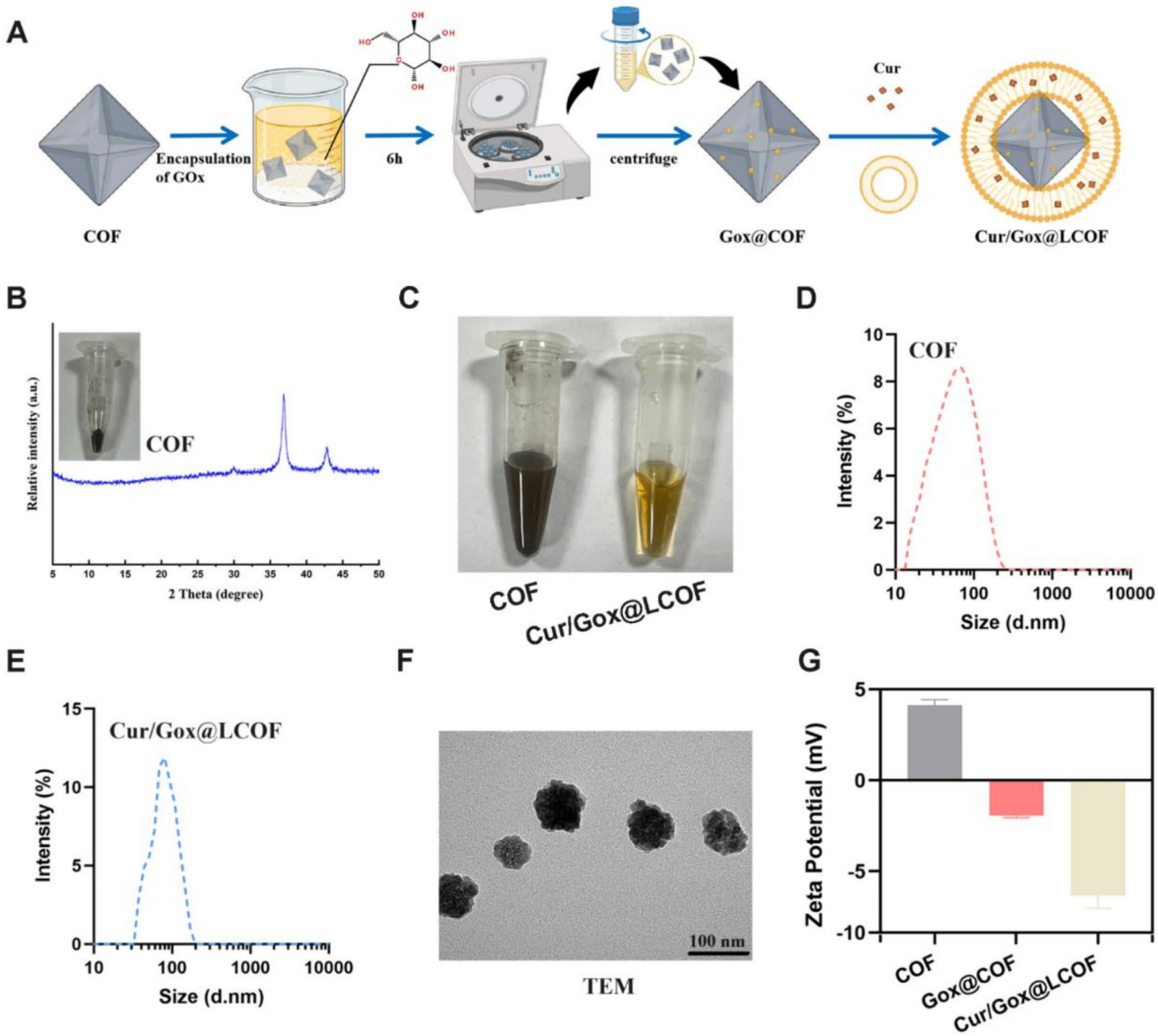

Fig. 2. (**A**) Schematic illustration of the design and synthesis of Cur/Gox@LCOF. (**B**) XRD pattern of COF. (**C**) Optical images of Gox@LCOF. (**D**) Hydrodynamic particle size distribution of COF. (**E**) Hydrodynamic particle size distribution of Cur/Gox@LCOF. (**F**) TEM morphology of Cur/Gox@LCOF. (**G**) Zeta potential measure-ment of Cur/Gox@LCOF.

Drug release studies

This study investigated the drug release behavior of Cur/Gox@LCOF under varying pH conditions, specifically pH 7.4 and pH 5.0, to simulate the physiological environment of normal tissues and the acidic microenvironment of tumors, respectively[22]. As illustrated in Fig. 3D, Cur release from the Cur/Gox@LCOF nanosystem remained minimal at physiological pH (7.4), with a cumulative release of approximately 20% over 48 h. In contrast, under acidic conditions (pH 5.0), a significantly enhanced release was observed, reaching 68.2% within the same period. A similar pH-responsive release pattern was noted for GOx (Fig. 3E), where 68.5% of GOx was released at pH 5.0 after 24 h, compared to only 27.1% at pH 7.4. These results demonstrate the pH-sensitive drug release characteristics of Cur/Gox@LCOF, enabling targeted drug release within the acidic tumor microenvironment, thereby enhancing therapeutic efficacy while reducing systemic toxicity. The observed pH-responsive release behavior of Cur/Gox@LCOF can be attributed to the acid-sensitive degradation of its copper-based metal-organic framework (COF). In acidic environments, the coordination between copper ions and the ligands in the framework may be disrupted, leading to the disassembly of the structure or the release of copper ions, which subsequently accelerates drug release[23]. This mechanism enables Cur/Gox@LCOF to achieve targeted and efficient drug delivery within the tumor's acidic microenvironment while limiting the impact on healthy tissues. Existing studies also confirm that metal-organic frameworks (MOFs) exhibit low structural stability under acidic conditions and pronounced pH-responsiveness, facilitating targeted drug release at tumor sites[24,25].

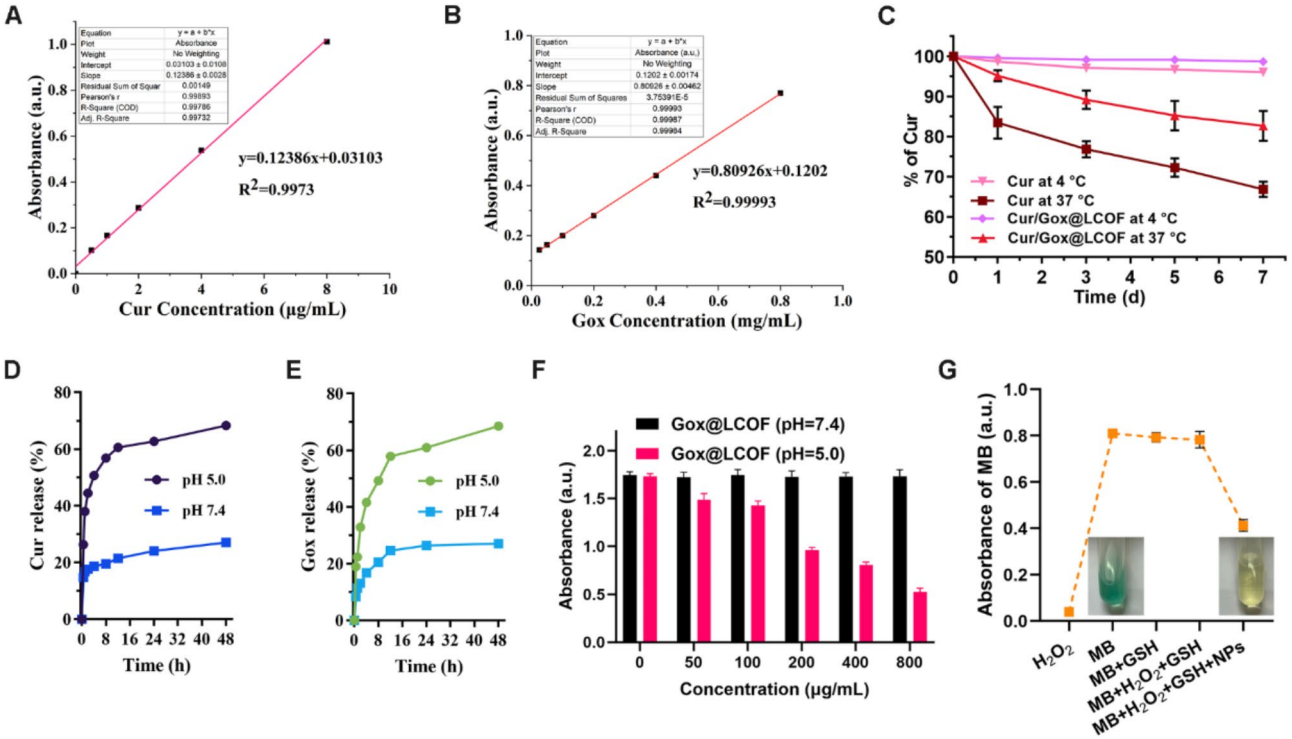

Fig. 3. (**A**) In vitro UV-vis standard curve of Cur. (**B**) Standard curve for determining the content of Gox by BCA protein quantification method. (**C**) Stability test for Cur and Cur/Gox@LCOF at 4 ℃ and 37 ℃. (**D**) Release profile of Cur in Cur/Gox@LCOF NPs. (**E**) Relative amount of GOx released from Cur/Gox@LCOF NPs. (**F**) Gox@LCOF–mediated GSH depletion, measured by the 5,5′-dithiobis-(2-nitrobenzoic acid) (DTNB) assay. (**G**) Assessment of Gox@LCOF–catalyzed Fenton-like reaction. The MB assay was used to examine the catalytic capability of Gox@LCOF in promoting the Fenton-like reaction.

Therefore, the pH-sensitive release characteristics of Cur/Gox@LCOF provide strong evidence for its potential in tumor-targeted therapy and offer promising prospects for enhancing the therapeutic efficacy and bioavailability of Cur-based treatments.

GSH and MB depletion

GSH serves not only as an endogenous reactive oxygen species (ROS) scavenger but also as a critical chaperone for intracellular copper ions, facilitating the protection of cancer cells from oxidative damage[26]. Consequently, the rapid depletion of GSH has emerged as a promising strategy for disrupting cellular redox equilibrium[27]. The Cur/Gox@LCOF complex demonstrates efficient intracellular delivery of Cu^{2+}, thereby promoting ROS generation and directly depleting GSH. This approach holds considerable potential as a therapeutic modality for cancer treatment. In this study, we comprehensively evaluate the GSH-scavenging capacity of Cur/Gox@LCOF. To assess this, we utilized the DTNB (5,5'-dithio-2,2'-dinitrobenzoic acid) reagent, a widely employed compound in biochemistry and molecular biology due to its high reactivity with thiol (–SH) groups. Upon interaction with free SH groups in the sample, DTNB is converted to TNB (2-nitro-5-thiobenzoic acid), which exhibits a characteristic absorbance at 412 nm. The intensity of TNB absorbance is directly proportional to the concentration of free SH groups in the sample. As shown in Fig. 3F, under acidic conditions (pH 5.0), a positive correlation is observed between the concentration of Gox@LCOF and its GSH consumption ability; specifically, higher material concentrations result in a weaker absorbance at 412 nm, confirming the effective GSH depletion by Gox@LCOF. Notably, under neutral conditions (pH 7.4), no significant change in TNB absorbance was observed with increasing Gox@LCOF concentration, further corroborating the pH-sensitive degradation behavior of Gox@LCOF in neutral environments.

The generation of •OH by Cur/Gox@LCOF is critical to the efficacy of CDT. In this study, methylene blue (MB), a compound that undergoes degradation in the presence of •OH, was employed as an indicator for •OH generation[28]. Upon exposure to •OH, MB undergoes gradual degradation, resulting in a reduction of its UV absorbance at 660 nm, accompanied by a shift in the solution color from blue to colorless. As illustrated in Fig. 3G, the MB in the control group retains its blue color and exhibits strong absorbance, whereas the Gox@LCOF group shows a significant fading of color and a marked reduction in absorbance, indicating the substantial catalytic activity of Gox@LCOF in facilitating the Fenton reaction. This observed catalytic behavior facilitates the oxidation and degradation of MB, suggesting the potential for Cur/Gox@LCOF to generate H_2O_2 in vivo, thereby enhancing the efficacy of CDT.

In vitro cytotoxicity and cellular uptake

To demonstrate the synergistic therapeutic effect of the prepared Cur/Gox@LCOF on cancer cell lethality via CDT/chemotherapy/starvation therapy, the inhibitory effect of Cur/Gox@LCOF on breast cancer was evaluated in vitro using 4T1 cells. As shown in Fig. 4A and B, LCOF showed negligible cytotoxicity against 4T1 cells, indicating that LCOF has excellent biocompatibility and can be used as a good nanocarrier-loaded drug. Both Cur and Cur@LCOF inhibited the viability of 4T1 cells to some extent. The decrease in cell viability was greater in the Cur@LCOF group than in the Cur group. This proved that Cur@LCOF could fully exert the synergistic anti-tumor effect of CDT and chemotherapy, further indicating that the anti-tumor effect of synergistic treatment was superior to that of monotherapy. The cell viability of Cur/Gox@LCOF was the lowest among all groups. This indicated that the addition of Gox had a good therapeutic effect on starvation therapy in 4T1; at the same time, the cell viability of cancer cells was significantly suppressed by the combination of generated H_2O_2 with enhanced CDT and starvation therapy and chemotherapy. These results suggest that Cur/Gox@LCOF can effectively kill tumor cells in vitro in combination with CDT, chemotherapy, and starvation therapy.

To investigate the cellular uptake kinetics of Cur/Gox@LCOF, the green fluorescence property of Cur was exploited and visualized by inverted fluorescence microscopy[29]. After incubation for 1 h, 2 h, and 4 h, significant green fluorescence was observed in 4T1 cells (Fig. 4C), and the fluorescence intensity gradually increased with time. Nevertheless, Fig. 4D shows the mean fluorescence intensity (MFI) of Cur quantified by Image J. Compared with 1 h and 2 h, there was a significant difference ($p < 0.01$) in the 4 h group, proving that the cells had a high uptake rate of Cur/Gox@LCOF, which gradually accumulated in the cells with time. The intracellular distribution of Cur/Gox@LCOF in 4T1 cells was also analyzed using CLSM, as shown in Fig. 4E. Following a 4-hour incubation with Cur/Gox@LCOF under identical conditions, the cells were sequentially stained with Hoechst 33342 and Lyso-Tracker Green to label the nuclei and lysosomes, respectively. CLSM imaging revealed that the nuclei emitted blue fluorescence, lysosomes exhibited red fluorescence, and Cur/Gox@LCOF displayed green fluorescence. These findings confirm the effective cellular uptake of the nanoparticles and their well-defined intracellular distribution.

Determination of intracellular ROS and GSH in tumor cells

The core mechanism of chemokinetic therapy involves the induction of apoptosis in tumor cells by catalyzing the conversion of H_2O_2 into highly reactive hydroxyl radicals (•OH) through Fenton or Fenton-like reactions. To further investigate this process, we assessed the chemokinetic activity of Cur/Gox@LCOF nanoparticles at the cellular level using a DCFH-DA probe. Upon oxidation by ROS, DCFH-DA is converted to 2′,7′-dichlorofluorescein (DCF), which emits green fluorescence at a wavelength of 525 nm[30]. This allowed for the visualization and quantification of intracellular ROS levels. As shown in Fig. 5A and B, the fluorescence intensity in both the control and LCOF groups was relatively weak, suggesting that although ROS levels in cancer cells were upregulated, the increase was modest. In contrast, significant enhancement of green fluorescence was observed in the Cur, Gox, Cur/Gox, and Cur@LCOF treatment groups, indicating that these treatments effectively stimulated the generation of substantial amounts of ROS within the cells. Notably, the ROS levels

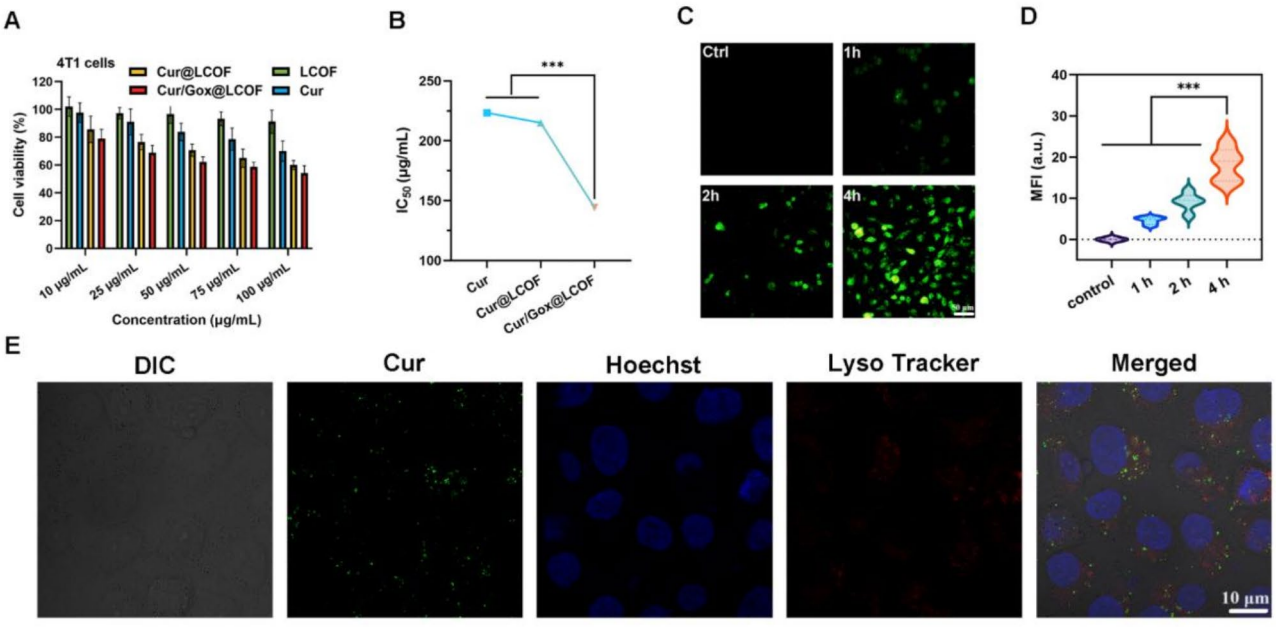

Fig. 4. (**A**) Cell viability of Cur/Gox@LCOF with 4T1 cells after 24 h incubation; (**B**) The corresponding half maximal inhibitory concentration (IC_{50}) of (**A**). (**C**) Intracellular uptake of Cur/Gox@LCOF in 4T1 cells for 1, 2, 4 h. (**D**) Quantification of fluorescence intensity of 4T1 cells ($n = 5$). (**E**) CLSM images of 4T1 cells in terms of the subcellular distribution of the Cur/Gox@LCOF.

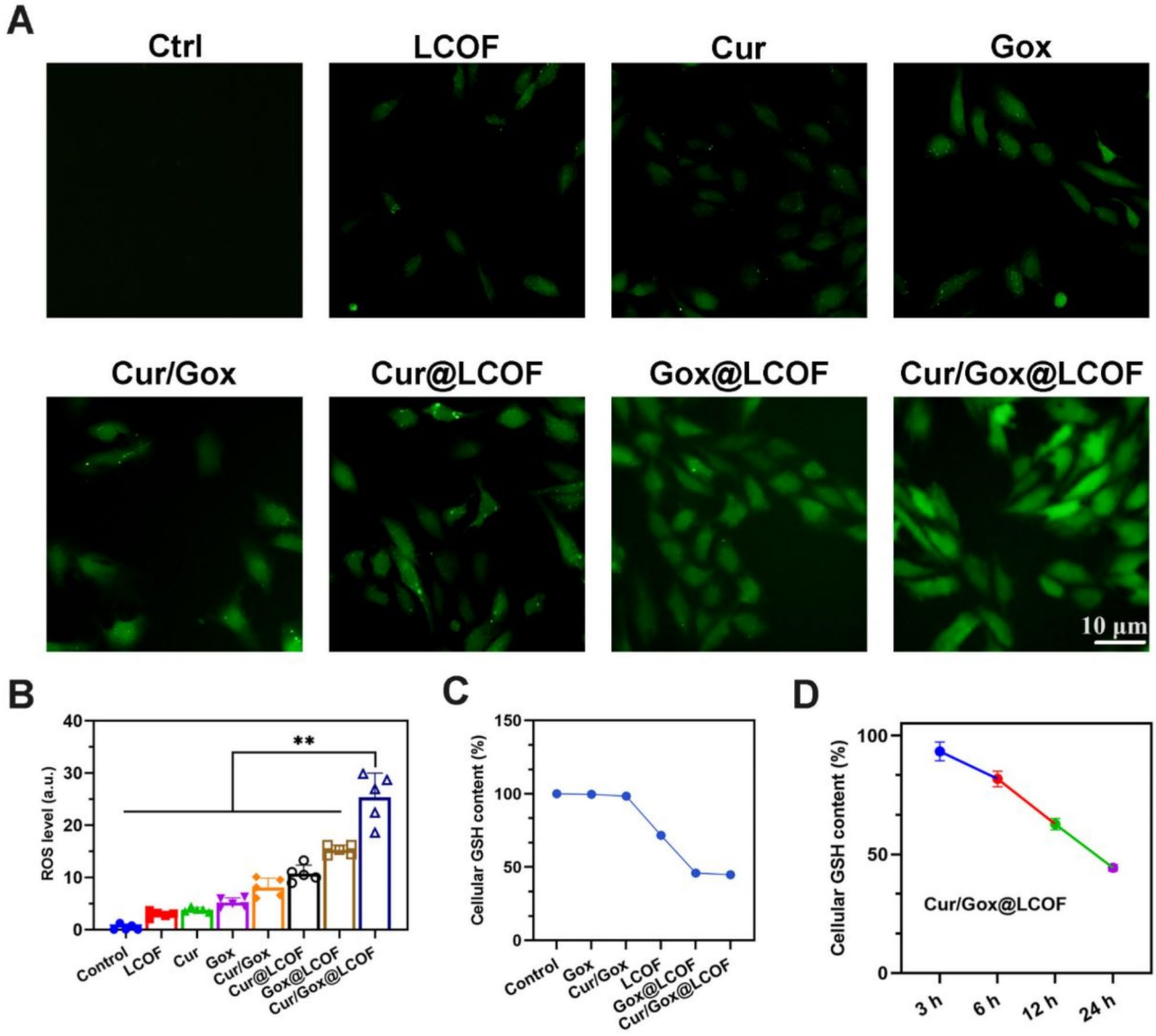

Fig. 5. (**A**) Intracellular ROS levels (measured microscopically in response to DCF fluorescence intensity) in 4T1 cells treated with different drugs. Non-treated cells were used as controls. (**B**) Quantification of intracellular ROS fluorescence intensity in 4T1 cells. (**C**) GSH levels of 4T1 cells incubated with different drugs for 24 h. (**D**) GSH levels of 4T1 cells incubated with Cur/Gox@LCOF for various time periods.

in the Gox@LCOF group were markedly higher than those in the Cur/Gox@LCOF group. This difference was primarily attributed to the presence of Gox, which specifically degrades glucose within tumor cells, generating a large amount of H_2O_2. This process resulted in a pronounced green fluorescence, reflecting a significant increase in ROS levels. These findings not only confirm that the LCOF carrier exhibits superior chemokinetic activity, but also demonstrate that Cur/Gox@LCOF nanoparticles effectively enhance ROS generation specifically within the tumor microenvironment. This supports the potential of chemokinetic therapies in cancer treatment, highlighting their considerable promise as a potent therapeutic strategy for tumors.

Subsequently, monobromodiamine (mBBr), a sulfhydryl-specific fluorescent probe, was employed to quantify intracellular GSH levels in 4T1 cells subjected to various treatments. The Cu^{2+} ions released from the COF interacted with intracellular GSH in a redox reaction, leading to GSH consumption and the conversion of Cu^{2+} to Cu^{+} ions. This Cu^{+} ion then catalyzed the formation of highly cytotoxic •OH via a Fenton-like reaction. The intracellular GSH content was assessed by measuring the fluorescence intensity of the mBBr-GSH adduct. Following 24 h of incubation (Fig. 5C), the fluorescence intensity of the PBS-treated control cells was set at 100% as a reference. The fluorescence intensity in the Cur and Cur/Gox treatment groups showed minimal change, suggesting a weak depletion of intracellular GSH. In contrast, the LCOF-treated group exhibited a decrease in fluorescence intensity, indicating a moderate effect on GSH, while the Gox@LCOF and Cur/Gox@LCOF groups showed a more significant reduction in fluorescence intensity, reflecting a more substantial depletion of intracellular GSH. To further explore the dynamics of intracellular GSH consumption, the fluorescence intensity

was measured at 3, 6, 12, and 24 h post-incubation. The results revealed a clear, time-dependent decrease in fluorescence intensity (Fig. 5D), confirming that Cur/Gox@LCOF nanoparticles continuously deplete intracellular GSH over time. These findings, in conjunction with prior MTT-based in vitro cytotoxicity assays and ROS level measurements, indicate that the changes in intracellular GSH levels are closely linked to cell viability and ROS accumulation. The Cu^{2+} ions released from Cur/Gox@LCOF nanoparticles consume GSH and generate •OH, which facilitate the buildup of ROS within cells. This accumulation of ROS exacerbates oxidative stress, thereby significantly increasing cellular toxicity.

In vivo anti-tumor efficacy

Encouraged by the excellent in vitro results, we then evaluated the synergistic therapeutic effect of Cur/Gox@LCOF in 4T1 tumor-bearing mice (Fig. 6A). Throughout the 14-day treatment period, tumor volume and body weight were monitored every two days, accompanied by histological and survival analyses. Body weight monitoring (Fig. 6B) revealed no significant weight loss across treatment groups, highlighting the favorable biosafety profile of Cur/Gox@LCOF. Tumor growth monitoring (Fig. 6C) demonstrated that Cur/Gox@LCOF treatment significantly suppressed tumor progression compared to the control group ($P < 0.05$). After treatment (day 14), mice in the Cur/Gox@LCOF group exhibited the smallest tumor volumes and the lowest average tumor weight among all groups (Fig. 6D). Moreover, during the 60-day observation period, the survival rate of mice treated with Cur/Gox@LCOF was markedly higher than that of other groups (Fig. 6E), underscoring the system's potential to effectively alleviate tumor burden and improve therapeutic outcomes. Histopathological analysis corroborated these findings. H&E staining (Fig. 6F) revealed pronounced nuclear condensation, fragmentation, and dissolution in the tumor tissues of the Cur/Gox@LCOF-treated group, indicative of extensive tumor cell apoptosis. In contrast, tumor sections from the PBS control group retained more intact cellular morphology. Furthermore, Ki-67 staining (Fig. 6F) confirmed that Cur/Gox@LCOF significantly suppressed tumor cell proliferation. As a lipid-modified COF nanocarrier, Cur/Gox@LCOF demonstrated excellent biocompatibility and robust drug-loading capacity. Its accumulation within tumor tissues was facilitated by the enhanced permeability and retention (EPR) effect[31,32]. Future investigations may integrate tumor-specific targeting ligands, such as tumor-associated antibodies or peptide molecules, to further augment its targeted drug delivery and therapeutic efficiency.

In summary, Cur/Gox@LCOF integrates the synergistic modalities of chemotherapy, CDT, and tumor starvation therapy. The release of GOx catalyzes glucose oxidation to produce hydrogen peroxide, which subsequently generates hydroxyl radicals via endogenous Fe^{2+}, inducing oxidative damage and tumor cell apoptosis. Additionally, the incorporation of Cur not only enhances apoptotic activity but also provides antioxidant and anti-inflammatory effects, offering additional potential for modulating the tumor microenvironment. This multimodal therapeutic strategy effectively overcomes the limitations of monotherapy, resulting in significantly enhanced anti-tumor efficacy.

In vivo toxicity study

An optimal nano-drug delivery system should not only demonstrate potent therapeutic efficacy but also minimize adverse effects to an insignificant level[33]. Therefore, it is crucial to thoroughly evaluate the side effects and potential systemic toxicity of Cur/Gox@LCOF during treatment. The biocompatibility of Cur/Gox@LCOF was evaluated using four key parameters: hemolysis assay, histological examination of major organs (heart, liver, spleen, lung, kidney) by H&E staining, analysis of routine blood parameters from mouse orbital blood, and assessment of serum biochemical indices. Initially, blood compatibility was assessed using a hemolysis assay, with results (Fig. 7A) showing that the hemolysis rate of Cur/Gox@LCOF remained below 5.0% over the concentration range of 1–100 μg/mL, indicating favorable blood compatibility. Further analysis of routine blood parameters and standard biochemical indices was performed, including hematological indicators such as white blood cell count (WBC), red blood cell count (RBC), and hemoglobin (HGB); liver toxicity markers including alanine aminotransferase (ALT), aspartate aminotransferase (AST) and alkaline phosphatase (ALP); and renal function indicators including creatinine (CREA), uric acid (UA) and blood urea nitrogen (BUN). The data (Fig. 7B and G) showed no significant differences in these indices between the different treatment groups, highlighting the favorable biocompatibility of Cur/Gox@LCOF and the absence of significant adverse effects on the normal physiological growth of the mice. To further investigate potential systemic toxicity, mice were euthanized on day 14 of treatment, and histopathology was performed on the major organs of mice from each treatment group. The results (Fig. 7H) showed no significant changes in the tissue morphology of the major organs, with no evidence of tissue damage or inflammatory infiltration. This observation indicates that Cur/Gox@LCOF does not induce damage to major organs, further supporting its excellent biocompatibility and safety profile.

In conclusion, Cur/Gox@LCOF effectively inhibits tumor growth through the synergistic effects of chemotherapy, CDT, and starvation therapy, while exhibiting superior biocompatibility. This makes it a promising candidate for the advancement of cancer therapy.

Materials and methods

Materials

Curcumin (Cur), copper(II) chloride dihydrate ($CuCl_2{\cdot}2\ H_2O$), sodium hydroxide (NaOH), ascorbic acid, 1,3,5-benzenetricarboxylic acid (H_3BTC), and polyvinylpyrrolidone (PVP) were obtained from Shanghai McLean Biochemical Technology Co., Ltd. (China). The MTT assay kit was purchased from Biyuntian Biotechnology Co., Ltd. (China). Dipotassium hydrogen phosphate, potassium dihydrogen phosphate, and dimethyl sulfoxide (DMSO) were supplied by Shanghai Sinopharm Chemical Reagent Co., Ltd. (China). Methanol (HPLC grade)

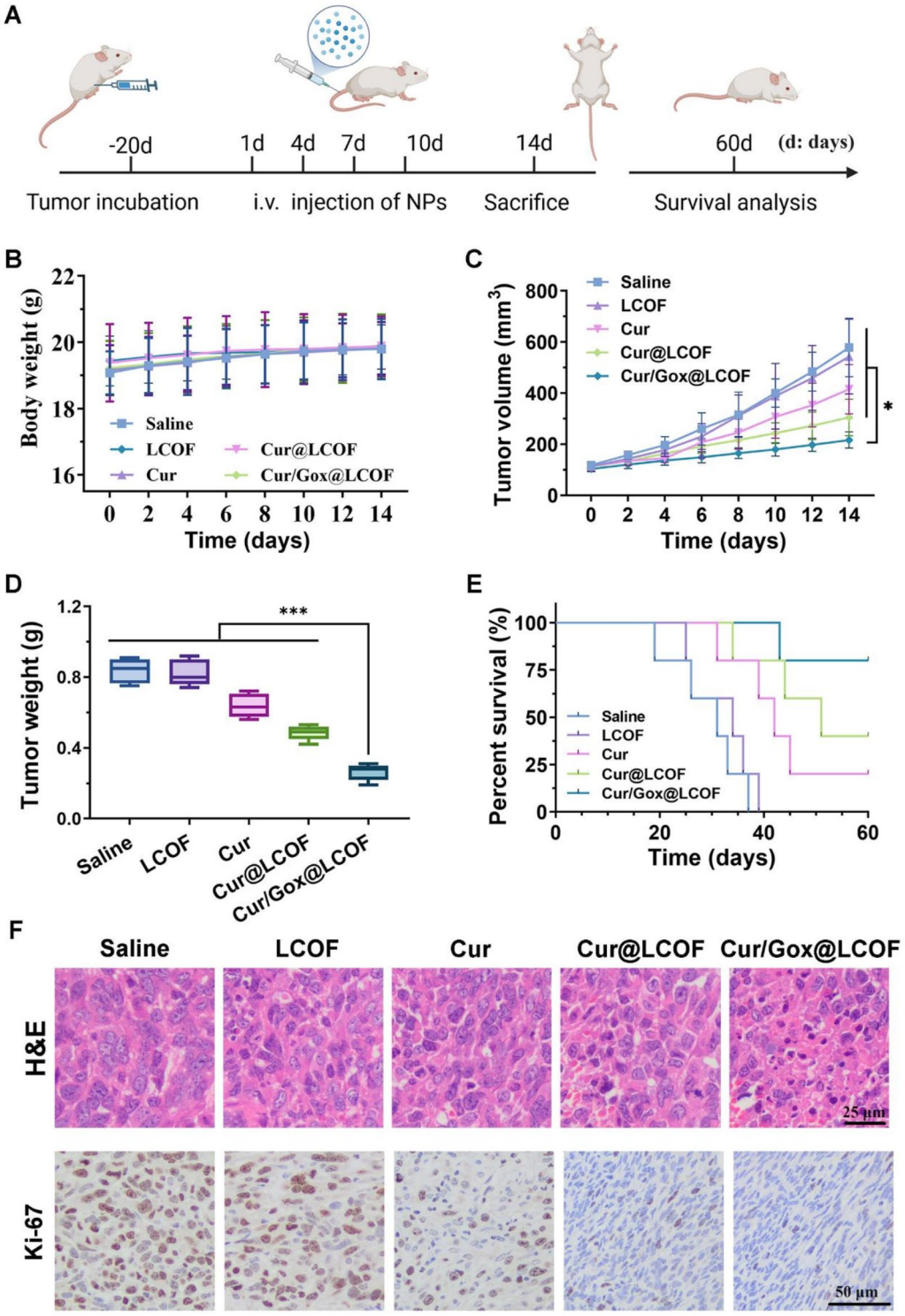

Fig. 6. Evaluation of in vivo anti-tumor capabilities of Cur/Gox@LCOF. (**A**) Therapeutic protocol illustrating Cur/Gox@LCOF administration. (B) Body weight fluctuations of 4T1 tumor-bearing mice over the 14-day treatment span. (**C**) Tumor growth trajectories in 4T1 tumor-bearing mice post-Cur/Gox@LCOF treatment. Tumor progression was monitored over 14 days. (**D**) The average tumor weight after 14 days of treatment. (**E**) Survival tracking of tumor-bearing mice throughout the 60-day treatment in each group. (**F**) H&E and Ki-67 staining images of the dissected tumor tissues after 14 days of treatment.

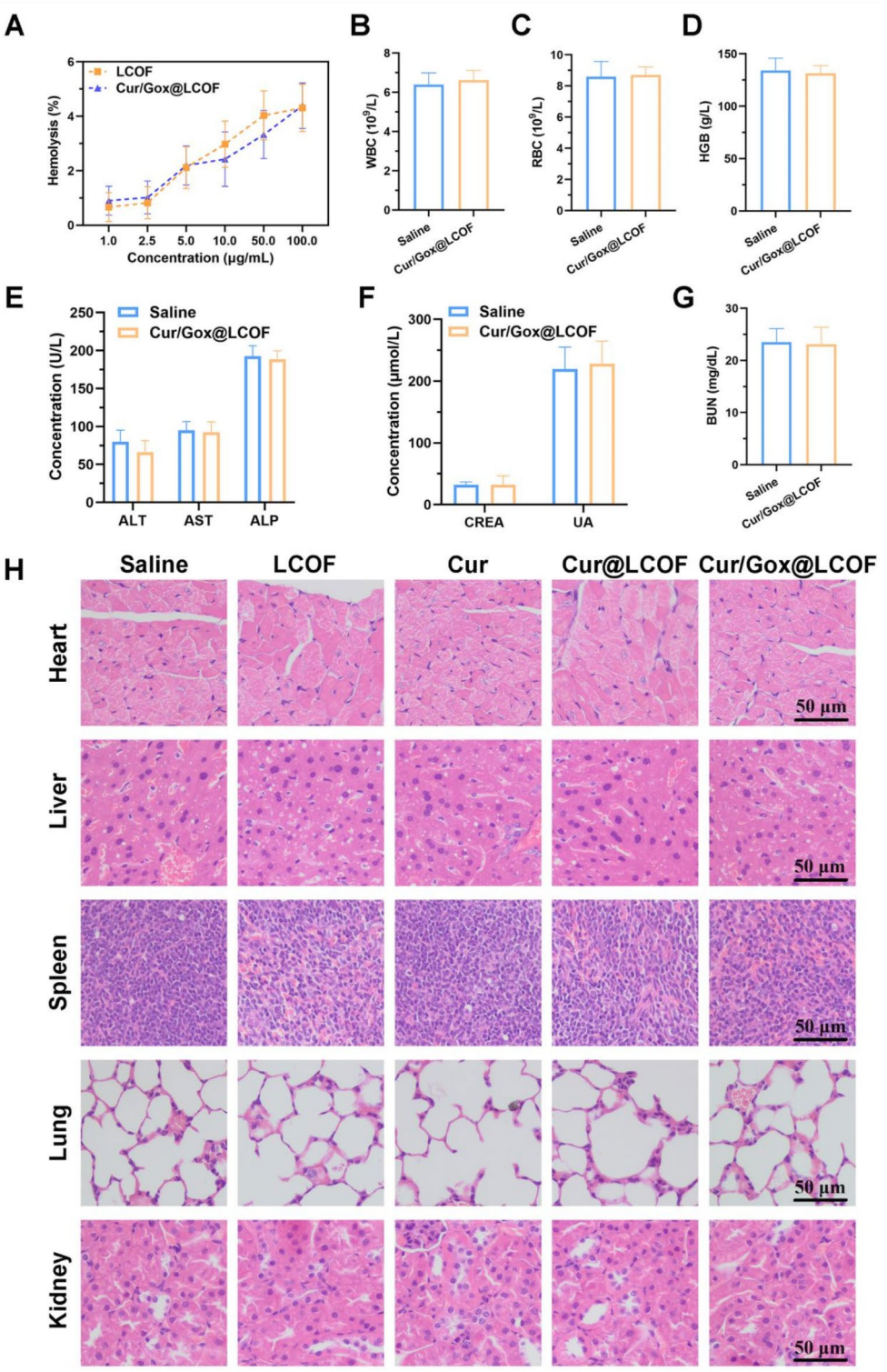

Fig. 7. The safety analysis of Cur/Gox@LCOF. (**A**) Hemolysis analysis of Cur/Gox@LCOF. (**B**-**G**) Blood routine and blood biochemistry results of mice treated with Cur/Gox@LCOF. (**H**) H&E staining images of dissected major organs (heart, liver, spleen, lung, kidney) of 4T1 tumor-bearing mice after various treatments for 14 days by intravenous administration.

was procured from Xilong Chemical Co., Ltd. (China). All water used in the experiments was double-distilled water.

Cell lines and animals

Mouse-derived breast cancer 4T1 cells were purchased from the Chinese Academy of Sciences cell bank (Shanghai, China). The cells were cultured in DMEM medium supplemented with 10% fetal bovine serum and 1% penicillin/streptomycin, and maintained at 37 ℃ in a humidified atmosphere containing 5% CO_2. The animals in this work were 6- to 8-week-old healthy female mice (18–22 g, BALB/c) purchased from Liaoning Changsheng Biotechnology Co., Ltd (Benxi, China).

Preparation of Cur/Gox@LCOF

Preparation of copper-based nMOFs (COF)

COF was synthesized using a modified one-step solvothermal reduction method, based on previously reported protocols[13,14,34]. Initially, 3.5 g of polyvinylpyrrolidone and 0.56 g of cupric chloride were dissolved in 100 mL of deionized water. Subsequently, 7.5 mL of sodium hydroxide solution (2 M) was added dropwise under constant stirring. After 5 min of stirring, 7.5 mL of ascorbic acid solution (1 M) was gradually introduced into the mixture. Following an additional 5 min of stirring, the resultant product was collected by centrifugation, washed twice with ethanol, and dried to yield yellow copper oxide nanoparticles. These nanoparticles were then redispersed in 20 mL of ethanol, to which 20 mL of N, N-dimethylformamide (DMF) solution was added. After a 4-hour reaction at room temperature, the resulting COF was separated by centrifugation, thoroughly washed with ethanol, and stored for further use.

Preparation of Gox@COF

For the encapsulation of GOx, 100 mg of COF dispersion was incubated with 10 mg of GOx at 4 °C for 6 h. Subsequently, the mixture was centrifuged to remove unencapsulated GOx. The resulting GOx-loaded COF (Gox@COF) was collected and stored for further use.

Preparation of Cur/Gox@LCOF

To prepare Cur/Gox@LCOF, 100 mg of lecithin, 25 mg of cholesterol, 25 mg of Cur, and 50 mg of Gox@COF were accurately weighed and dissolved in 10 mL of ethanol. The solution was then mixed with 40 mL of PBS buffer (pH 6.4) and stirred at 35 °C in a water bath for 6 h. The mixture was subsequently ultrasonicated at 450 W for 10 min using a pulse mode (3 s on, 3 s off) to obtain the final Cur/Gox@LCOF formulation.

Characterization of Cur/Gox@LCOF

A comprehensive structural analysis of COF was conducted using X-ray powder diffraction (XRD) within a scanning range of 5° to 60°, providing the characteristic diffraction pattern of the material. The morphology and particle size of Cur/Gox@LCOF were examined via TEM. DLS measurements (Zetasizer Nano ZS, Malvern Instruments Limited, UK) were performed at 25 °C to determine the hydrodynamic diameter and zeta potential of the freshly prepared Cur/Gox@LCOF. The drug loading efficiency was determined via UV–vis spectroscopy by measuring the absorbance of Cur at 430 nm, based on a pre-established standard calibration curve. The concentration of Gox was quantified using the bicinchoninic acid (BCA) protein assay kit.

In vitro stability and drug release

Cur/Gox@LCOF and free Cur were individually dispersed in phosphate-buffered saline (PBS) to evaluate the stability of Cur/Gox@LCOF. The stability tests were conducted at 4 °C and 37 °C for 7 days. Absorbance measurements were taken at various time intervals, and the Cur content was quantified. Each measurement was performed in triplicate to ensure the accuracy and reproducibility of the results.

The release profile of Cur/Gox@LCOF was evaluated at pH 5.0 and 7.4 using a release medium consisting of phosphate-buffered saline (PBS) containing 0.5% Tween-80 and 25% (v/v) ethanol[35]. A precise amount of Cur/Gox@LCOF was weighed and mixed with an equal volume of the release medium. The mixture was then placed in a pre-treated dialysis bag (molecular weight cutoff range of 8000–14000 Da). The dialysis bag was submerged in 100 mL of release medium, and the release study was conducted at 37 ℃ with continuous stirring at 100 rpm. To ensure experimental consistency, 2 mL samples were withdrawn at predetermined time intervals (0.5, 1, 2, 4, 8, 12, 24, and 48 h), and the same volume of release medium was replenished. The absorbance of the samples was measured using a UV-visible spectrophotometer, and the cumulative release of Cur was calculated. Similarly, Gox was quantitatively analyzed by the BCA protein assay method[36]. The resulting data were used to construct an in vitro release curve, providing insight into the release kinetics of Cur/Gox@LCOF.

GSH depletion

To assess the GSH scavenging capacity of Gox@LCOF, 5,5′-dithiobis-(2-nitrobenzoic acid) (DTNB) was employed as a probe to monitor the catalytic interaction between Gox@LCOF and GSH through the colorimetric reaction of DTNB with GSH[37]. Glutathione solutions (10 mM) were incubated with varying concentrations of Gox@LCOF (0, 50, 100, 200, 400, and 800 μg/mL) in PBS at pH 5.0 and 7.4 at 37 ℃ under dark conditions for 12 h. Subsequently, DTNB (2.5 mg/mL) was added, and the mixtures were incubated at 37 ℃ for an additional 10 min. The UV absorbance of the reaction products was measured at 412 nm.

In vitro chemical kinetic performance testing

To assess the catalytic efficiency of Cur/Gox@LCOF in Fenton and Fenton-like reactions, MB was employed as a spectrophotometric indicator. The experimental procedure involved adding 20 μL of 1 mg/mL MB solution,

20 μL of H_2O_2 solution (1 M), 20 μL of 10 mM glutathione aqueous solution, and a specific amount of Gox@LCOF nanoparticles (at a concentration of 800 μg/mL) to 2 mL of phos-phate-buffered saline (pH 5.0, 10 mM). Following incubation at 37 ℃ for 12 h, the reaction mixture was centrifuged, and the supernatant was collected. The absorbance of MB was then measured at 660 nm using a UV-Vis spectrophotometer[37]. A control group, in which H_2O_2 was omitted, was included for comparison.

Cytotoxicity test

In this study, 4T1 cells were utilized as a model to evaluate the effects of various treatments. To assess cell viability, 4T1 cells were seeded in 96-well plates at a density of 6×10^3 cells per well. After a 12-hour incubation, the medium was removed and replaced with fresh medium containing varying concentrations of nanoparticles (0, 25, 50, 75, and 100 μg/mL). The cells were then incubated for an additional 24 h under the same conditions. The experimental groups included PBS, LCOF, Cur, Cur@LCOF, and Cur/Gox@LCOF. After 24 h of incubation at 37 ℃ and 5% CO_2, 10 μL of MTT solution was added to each well. Following a 2-hour incubation period, formazan crystals were solubilized in DMSO, and the absorbance was measured at 570 nm.

Cellular uptake in 4T1 cells

4T1 cells (1×10^5 cells per well) were seeded in 24-well plates and incubated overnight at 37 °C. Following this, the original culture medium was removed, and the cells were treated with complete medium containing Cur/Gox@LCOF for 1, 2, or 4 h. At each designated time point, the drug-containing medium was replaced, and the cells were washed three times with PBS. Fluorescence microscopy was subsequently employed to observe the cellular uptake of the nanoparticles.

To gain a more precise understanding of the intracellular distribution of the Cur/Gox@LCOF nanocarriers, 4T1 cells were treated with Cur/Gox@LCOF for 4 h under the same conditions. After incubation, the cells were stained with Hoechst 33342 (10 μg/mL) for 15 min to label the nuclei, followed by a 30-minute incubation with Lyso-Tracker Green (1 mM) to label the lysosomes. Confocal laser scanning microscopy (CLSM) was then utilized to visualize and assess the subcellular localization of Cur/Gox@LCOF nanoparticles within the cells.

Detection of intracellular ROS and GSH

The fluorescent probe DCFH-DA was used to determine the level of ROS production in cells after material treatment. 4T1 cells were inoculated into 24-well plates at a density of 1×10^5 cells/mL and cultured overnight in an incubator until the cells were adherent. The cells were treated with PBS, LCOF, Cur, Cur@LCOF, Gox@LCOF, and Cur/Gox@LCOF. After 24 h of co-culture, the drug-containing medium was discarded, PBS was washed three times, and the cells were stained with DCFH-DA (at a concentration of 10 μM) for 30 min at 37 ℃. The cells were then washed with serum-free DMEM and observed by inverted fluorescence microscopy.

Intracellular GSH levels were quantified using monobromobimane (mBBr) as a thiol-specific fluorescent probe[38]. Briefly, 4T1 cells were seeded in black 96-well plates at a density of 5×10^4 cells per well and incubated with 100 μL of culture medium for at least 12 h to allow cell attachment. Subsequently, the cells were treated with PBS, LCOF, Cur, Cur@LCOF, Gox@LCOF, and Cur/Gox@LCOF. Following a 24-hour incubation, cells were washed three times with Hanks' balanced salt solution (HBSS) and stained with 40 μM mBBr for 4 hours at 37 °C under dark conditions. The fluorescence intensity of the mBBr-GSH adduct was then measured using a microplate reader (excitation at 360 nm, emission at 465 nm). The fluorescence intensity of Cur/Gox@LCOF-treated cells was assessed at 3, 6, 12, and 24 h post-incubation to evaluate intracellular GSH levels. A reduction in fluorescence intensity corresponded to a decrease in intracellular GSH content. Fluorescence intensity in the PBS-treated control group (untreated cells) was designated as 100%, and the results were presented as the relative percentage of the experimental groups.

In vivo anti-tumor study

To establish a subcutaneous xenograft model, approximately 2×10^6 4T1 cells were subcutaneously injected into the right abdominal region of female BALB/c mice[35]. These mice were utilized for in vivo therapeutic efficacy and biosafety evaluations once the tumor volume reached approximately 100 mm^3. The anti-tumor efficacy of Cur/Gox@LCOF was assessed in 4T1 tumor-bearing mice through intravenous administration. The animals were randomly assigned to five experimental groups ($n = 5$ per group): (1) Saline (control), (2) LCOF, (3) Cur, (4) Cur@LCOF, and (5) Cur/Gox@LCOF. Each group received four intravenous injections of the respective formulations on days 1, 4, 7, and 10, with a Cur dose of 2 mg/kg per injection. Tumor size and body weight were monitored every two days throughout the treatment period. Tumor volume was calculated using the formula: volume = length × (width) $^2/2$, where length and width represent the longest and shortest dimensions of the tumor, respectively. On day 14, the mice were euthanized, and tumors along with major organs (heart, liver, spleen, lungs, and kidneys) were harvested for histological analysis using hematoxylin-eosin (H&E) staining. Tumor proliferative activity was further evaluated via Ki-67 immunohistochemical staining. In addition to these analyses, the survival rate of the animals was tracked over 60 days. All surgical procedures were performed under anesthesia (2% isoflurane). Method of euthanasia of mice: Cervical dislocation. Procedure: The operator held the tail of the nude mouse with the right hand, placed the mouse on the experimental table, held the head and neck of the mouse with the left hand, and applied force to pull the tail backward and upwards with the right hand. When the operator feels the spine separate, the animal dies immediately.

Hemolysis assay and blood biochemical index

Red blood cells (RBCs) were separated from serum by mixing 0.5 mL of whole blood with 1 mL of phosphate-buffered saline (PBS, pH 7.4), followed by centrifugation at 4500 rpm for 5 min. The isolated erythrocytes were washed five times with PBS to ensure purification and subsequently diluted to a final volume of 5 mL. From

the diluted erythrocyte suspension, 0.3 mL was carefully measured and mixed with 1.2 mL of PBS containing varying concentrations of LCOF or Cur/Gox@LCOF (LCOF concentrations ranging from 1 to 100 μg/mL). The mixture was vortexed to achieve homogeneity, gently shaken, and incubated at room temperature for 3 h. Following incubation, the samples were centrifuged, and the absorbance of the supernatant was recorded at 570 nm using a UV/Vis spectrophotometer. Deionized water-treated erythrocytes and PBS-treated erythrocytes served as positive and negative controls, respectively, to facilitate comparative analysis of hemolytic activity.

To assess blood biochemical parameters, healthy BALB/c mice were administered 100 μL of Cur/Gox@LCOF at a dose of 10 mg/kg via tail vein injection. Following 14 days of treatment, blood samples were collected from representative mice through enucleation and analyzed using a hematology analyzer. Mice receiving an equivalent dose of saline were used as the control group.

Statistical analysis

Microsoft Excel calculated the mean and standard deviation (SD). Data are presented as the mean ± SD. Statistical analyses were conducted using GraphPad Prism 9 software. Group differences were assessed using a two-sided Student's t-test or one-way ANOVA followed by Tukey's post hoc test. Statistical significance was determined as follows: ns, no significant difference; $^{*}P < 0.05$; $^{**}P < 0.01$; $^{***}P < 0.001$; $^{****}P < 0.0001$.

Conclusions

In this study, we report the design and synthesis of a novel curcumin and glucose oxidase-based drug delivery nanosystem (Cur/Gox@LCOF), which exploits the structural advantages of COFs for efficient drug encapsulation and controlled release. The Cur/Gox@LCOF nanosystem integrates multiple therapeutic modalities, including chemotherapy, CDT, and tumor starvation therapy, resulting in enhanced anti-tumor efficacy through a series of cascade reactions. Notably, the synergistic effects of Cur/Gox@LCOF in ROS generation, GSH depletion, and pH-responsive drug release underscore the novelty and potential clinical applicability of this approach. In vitro assays demonstrated that the Cur/Gox@LCOF nanosystem significantly enhanced ROS production and cytotoxicity in cancer cells while exhibiting excellent pH-responsive drug release profiles. The system's ability to generate ROS and deplete GSH within tumor cells, coupled with its pH-sensitive release behavior, contributes to its potent therapeutic efficacy and selectivity. In vivo studies further validated the system's robust anti-tumor activity and favorable biocompatibility, with significant tumor growth inhibition and improved survival rates in tumor-bearing mice. Future directions for this nanosystem include optimizing its design to further improve targeting specificity and therapeutic outcomes. The incorporation of tumor-specific targeting ligands, such as tumor-associated antibodies or peptides, could substantially enhance targeted drug delivery and therapeutic efficiency. Moreover, exploring the clinical potential of Cur/Gox@LCOF across various cancer types and assessing its long-term effects in larger animal models will be essential for advancing its translation into clinical settings. Overall, the Cur/Gox@LCOF nanosystem presents a promising multifunctional platform for cancer therapy, capable of synergistically combining chemodynamic, chemotherapy, and starvation therapies, thereby offering an effective strategy for enhanced cancer treatment.

Data availability

The datasets used and/or analysed during the current study available from the corresponding author on reasonable request.

Received: 18 January 2025; Accepted: 13 March 2025
Published online: 21 March 2025

References

1. Arnold, M. et al. Current and future burden of breast cancer: global statistics for 2020 and 2040. *Breast* **66**, 15–23. https://doi.org/10.1016/j.breast.2022.08.010 (2022).
2. Xu, H. & Xu, B. Breast cancer: epidemiology, risk factors and screening. *Chin. J. Cancer Res.* **35**, 565–583. https://doi.org/10.21147/j.issn.1000-9604.2023.06.02 (2023).
3. Khan, M. S. et al. Advancements in dextran-based nanocarriers for treatment and imaging of breast cancer. *Int. J. Pharm.* **643**, 123276. https://doi.org/10.1016/j.ijpharm.2023.123276 (2023).
4. Zheng, H. et al. A nanoreactor based on Metal-Organic frameworks with triple synergistic therapy for hepatocellular carcinoma. *Adv. Healthc. Mater.* **13**, e2401743. https://doi.org/10.1002/adhm.202401743 (2024).
5. Sandbhor, P., Palkar, P., Bhat, S., John, G. & Goda, J. S. Nanomedicine as a multimodal therapeutic paradigm against cancer: on the way forward in advancing precision therapy. *Nanoscale* **16**, 6330–6364. https://doi.org/10.1039/d3nr06131k (2024).
6. Wang, X., Zhong, X., Liu, Z. & Cheng, L. Recent progress of chemodynamic therapy-induced combination cancer therapy. *Nano Today*. **35**, 100946 (2020).
7. Zhang, L., Li, C. X., Wan, S. S. & Zhang, X. Z. Nanocatalyst-Mediated chemodynamic tumor therapy. *Adv. Healthc. Mater.* **11**, e2101971. https://doi.org/10.1002/adhm.202101971 (2022).
8. Tian, Q. et al. Recent advances in enhanced chemodynamic therapy strategies. *Nano Today*. **39**, 101162 (2021).
9. Fu, L. H. et al. Nanocatalytic theranostics with glutathione depletion and enhanced reactive oxygen species generation for efficient cancer therapy. *Adv. Mater.* **33**, e2006892. https://doi.org/10.1002/adma.202006892 (2021).
10. Yang, X. X. et al. A nanoreactor boosts chemodynamic therapy and ferroptosis for synergistic cancer therapy using molecular amplifier Dihydroartemisinin. *J. Nanobiotechnol.* **20**, 230. https://doi.org/10.1186/s12951-022-01455-0 (2022).
11. Huang, L. et al. Tumor-Generated reactive oxygen species storm for High-Performance ferroptosis therapy. *ACS Nano*. **17**, 11492–11506. https://doi.org/10.1021/acsnano.3c01369 (2023).
12. Wang, T. et al. Acidity-responsive cascade nanoreactor based on metal-nanozyme and glucose oxidase combination for starving and photothermal-enhanced chemodynamic antibacterial therapy. *Chem. Eng. J.* **446**, 137172 (2022).
13. Zhang, K., Meng, X., Yang, Z., Dong, H. & Zhang, X. Enhanced cancer therapy by hypoxia-responsive copper metal-organic frameworks nanosystem. *Biomaterials* **258**, 120278. https://doi.org/10.1016/j.biomaterials.2020.120278 (2020).

14. Ren, D. et al. Copper-Based Metal-Organic framework induces NO generation for synergistic tumor therapy and antimetastasis activity. *Small* **19**, e2205772. https://doi.org/10.1002/smll.202205772 (2023).
15. Li, L. et al. Triggered content release from optimized stealth thermosensitive liposomes using mild hyperthermia. *J. Control Release*. **143**, 274–279. https://doi.org/10.1016/j.jconrel.2010.01.006 (2010).
16. Pawar, N., Peña-Figueroa, M., Verde-Sesto, E., Maestro, A. & Alvarez-Fernandez, A. Exploring the interaction of lipid bilayers with Curcumin-Laponite nanoparticles: implications for drug delivery and therapeutic applications. *Small* **20**, e2406885. https://doi.org/10.1002/smll.202406885 (2024).
17. Beloqui, A., Solinís, M., Rodríguez-Gascón, A., Almeida, A. J. & Préat, V. Nanostructured lipid carriers: promising drug delivery systems for future clinics. *Nanomedicine* **12**, 143–161. https://doi.org/10.1016/j.nano.2015.09.004 (2016).
18. Taratula, O., Kuzmov, A., Shah, M., Garbuzenko, O. B. & Minko, T. Nanostructured lipid carriers as multifunctional nanomedicine platform for pulmonary co-delivery of anticancer drugs and SiRNA. *J. Control Release*. **171**, 349–357. https://doi.org/10.1016/j.jconrel.2013.04.018 (2013).
19. Can Karaca, A. et al. Lipid-based nanodelivery systems of Curcumin: recent advances, approaches, and applications. *Food Chem.* **463**, 141193. https://doi.org/10.1016/j.foodchem.2024.141193 (2025).
20. Hu, Q. & Luo, Y. Chitosan-based nanocarriers for encapsulation and delivery of Curcumin: A review. *Int. J. Biol. Macromol.* **179**, 125–135. https://doi.org/10.1016/j.ijbiomac.2021.02.216 (2021).
21. Mahjoubin-Tehran, M., Rezaei, S., Kesharwani, P. & Sahebkar, A. Nanospheres for Curcumin delivery as a precision nanomedicine in cancer therapy. *J. Biomater. Sci. Polym. Ed.* **35**, 2250–2274. https://doi.org/10.1080/09205063.2024.2371186 (2024).
22. Ji, P. et al. Hyaluronic acid-coated metal-organic frameworks benefit the ROS-mediated apoptosis and amplified anticancer activity of Artesunate. *J. Drug Target.* **28**, 1096–1109. https://doi.org/10.1080/1061186x.2020.1781136 (2020).
23. Liu, J. et al. pH-sensitive nano-systems for drug delivery in cancer therapy. *Biotechnol. Adv.* **32**, 693–710. https://doi.org/10.1016/j.biotechadv.2013.11.009 (2014).
24. Ruttala, H. B. & Ko, Y. T. Liposome encapsulated albumin-paclitaxel nanoparticle for enhanced antitumor efficacy. *Pharm. Res.* **32**, 1002–1016. https://doi.org/10.1007/s11095-014-1512-2 (2015).
25. Simon-Yarza, T. et al. A smart Metal-Organic framework nanomaterial for lung targeting. *Angew Chem. Int. Ed. Engl.* **56**, 15565–15569. https://doi.org/10.1002/anie.201707346 (2017).
26. Lu, Y., Pan, Q., Gao, W., Pu, Y. & He, B. Reversal of cisplatin chemotherapy resistance by glutathione-resistant copper-based nanomedicine via Cuproptosis. *J. Mater. Chem. B*. **10**, 6296–6306. https://doi.org/10.1039/d2tb01150f (2022).
27. Fu, J. et al. Activatable nanomedicine for overcoming hypoxia-induced resistance to chemotherapy and inhibiting tumor growth by inducing collaborative apoptosis and ferroptosis in solid tumors. *Biomaterials* **268**, 120537. https://doi.org/10.1016/j.biomaterials.2020.120537 (2021).
28. Zhou, R., Ohulchanskyy, T. Y., Xu, H., Ziniuk, R. & Qu, J. Catalase nanocrystals loaded with methylene blue as oxygen Self-Supplied, Imaging-Guided platform for photodynamic therapy of hypoxic tumors. *Small* **17**, e2103569. https://doi.org/10.1002/smll.202103569 (2021).
29. Zhao, Y. et al. A pH-triggered N-oxide polyzwitterionic nano-drug loaded system for the anti-tumor immunity activation research. *J. Nanobiotechnol.* **22**, 420. https://doi.org/10.1186/s12951-024-02677-0 (2024).
30. Li, Y. et al. MOF nanoparticles with encapsulated Dihydroartemisinin as a controlled drug delivery system for enhanced cancer therapy and mechanism analysis. *J. Mater. Chem. B*. **8**, 7382–7389. https://doi.org/10.1039/d0tb01330g (2020).
31. Chen, Z. A. et al. Receptor Ligand-Free mesoporous silica nanoparticles: A streamlined strategy for targeted drug delivery across the Blood-Brain barrier. *ACS Nano*. **18**, 12716–12736. https://doi.org/10.1021/acsnano.3c08993 (2024).
32. Ngo, T. L., Wang, K. L., Pan, W. Y., Ruan, T. & Lin, Y. J. Immunomodulatory prodrug micelles imitate mild heat effects to reshape tumor microenvironment for enhanced cancer immunotherapy. *ACS Nano*. **18**, 5632–5646. https://doi.org/10.1021/acsnano.3c11186 (2024).
33. Gou, S. et al. Multi-responsive nanotheranostics with enhanced tumor penetration and oxygen self-producing capacities for multimodal synergistic cancer therapy. *Acta Pharm. Sin B.* **12**, 406–423. https://doi.org/10.1016/j.apsb.2021.07.001 (2022).
34. Liu, L. et al. A copper-metal organic framework enhances the photothermal and chemodynamic properties of polydopamine for melanoma therapy. *Acta Biomater.* **158**, 660–672. https://doi.org/10.1016/j.actbio.2023.01.010 (2023).
35. Yan, Z. et al. Enhanced breast cancer therapy using multifunctional lipid-coated nanoparticles combining Curcumin chemotherapy and nitric oxide gas delivery. *Sci. Rep.* **14**, 18107. https://doi.org/10.1038/s41598-024-69229-2 (2024).
36. Fan, R. et al. Enhancing metformin-induced tumor metabolism destruction by glucose oxidase for triple-combination therapy. *J. Pharm. Anal.* **14**, 321–334 (2024).
37. Chen, K. et al. Cellular Trojan horse initiates bimetallic Fe-Cu MOF-mediated synergistic Cuproptosis and ferroptosis against malignancies. *Sci. Adv.* **10**, eadk3201. https://doi.org/10.1126/sciadv.adk3201 (2024).
38. Yang, C. et al. Oat protein-shellac nanoparticles as a delivery vehicle for Resveratrol to improve bioavailability in vitro and in vivo. *Nanomedicine* **14**, 2853–2871 (2019).

Author contributions

Conceptualization, P.J., and P.L.; methodology, Y.Y.S, Z.K.R., Z.R.Z., K.X.Y., Y.F.J., H.Y.D., Y.Z.L, J.L.W.; software, Y.Y.S.; validation, Z.R.Z.; formal analysis, P.L.; investigation, P.L.; resources, Z.K.R. and P.J.; writing—original draft preparation, Y.Y.S and Z.K.R; writing—review and editing, P.J., and P.L.; supervision, P.L.; project administration, Z.K.R. and P.J.; funding acquisition, Z.K.R. and P.J. All authors have read and agreed to the published version of the manuscript.

Funding

This work was supported by National Natural Science Foundation of China (32401196), Liaoning Provincial Science and Technology Programme Joint Programme (Natural Science Foundation Project) (2024-MSLH-155), Natural Science Foundation of Hangzhou (2024SZRYBH090001), Zhejiang Provincial Natural Science Foundation of China (LQ24H300001), Zhejiang Province Selected Funding for Postdoctoral Research Projects (ZJ2023083), Natural Science Foundation of Jiangsu Province for Universities (24KJB350011), Natural Science Foundation Project of Taizhou Science and Technology Support Programme (Social Development) (TS202402), Qinglan Project of Jiangsu Province of China (2024), Taizhou Fengcheng Yingcheng Talent Young Science and Technology Talent Support Project (2023), Taizhou University College Student Innovation and Entrepreneurship Training Program (cx250129y and cx250130y), Taizhou University 2025 Excellent Graduation Design (Thesis) Cultivation Program (No. 2025PY148).

Declarations

Ethics approval and consent to participate

All protocols and procedures related to animal sampling, care, and management were approved by the Jinzhou Medical University Animal Ethics Committee. All experiments and samplings were carried out using ethical and biosafety protocols approved by hospital guidelines. Besides, this study is reported by ARRIVE guidelines (https://arriveguidelines.org).

Competing interests

The authors declare no competing interests.

Informed consent statement

Not applicable.

Additional information

Correspondence and requests for materials should be addressed to P.J. or P.L.

Reprints and permissions information is available at www.nature.com/reprints.

Publisher's note Springer Nature remains neutral with regard to jurisdictional claims in published maps and institutional affiliations.